International Journal of Pharmaceutics 389 (2010) 223–231

Contents lists available at ScienceDirect

International Journal of Pharmaceutics

journal homepage: www.elsevier.com/locate/ijpharm

Pharmaceutical Nanotechnology

Preparation, characterization, and anticancer effects of simvastatin–tocotrienol lipid nanoparticles

Hazem Ali, Amit B. Shirode, Paul W. Sylvester, Sami Nazzal*

Department of Basic Pharmaceutical Sciences, College of Pharmacy, University of Louisiana at Monroe, Monroe, LA 71209-0497, United States

ARTICLE INFO

Article history:
Received 5 November 2009
Received in revised form 6 January 2010
Accepted 10 January 2010
Available online 1 February 2010

Keywords:
Nanoparticle
Tocotrienol
Simvastatin
Cancer therapy
Drug delivery

ABSTRACT

Previously it was shown that combined low dose treatment of tocotrienols and statins synergistically inhibited the growth of highly malignant +SA mammary epithelial cells in culture. Therefore, the objective of the present work was to prepare and characterize lipid nanoparticles that combined simvastatin and tocotrienol rich fraction (TRF) as potential anticancer therapy. The entrapment of simvastatin in the oily nanocompartments, which were formed by TRF inclusion into the solid matrix of the nanoparticles, was verified by its high entrapment efficiency and the absence of endothermic or crystalline peaks when blends were analyzed by DSC and PXRD, respectively. The release of simvastatin from the nanoparticles in sink conditions was characterized by an initial burst release of approximately 20% in 10 h followed by a plateau. No significant change in particle size (~100 nm) was observed after storage for six months. The anticancer activity of the nanoparticles was verified *in vitro* by observing their antiproliferative effects on malignant +SA mammary epithelial cells. The IC_{50} of the reference α-tocopherol nanoparticles was 17.7 μM whereas the IC_{50} of the simvastatin/TRF nanoparticles was 0.52 μM, which confirmed the potency of the combined treatment and its potential in cancer therapy.

1. Introduction

Statins represent a class of drugs that are widely used to lower blood cholesterol levels. However, recent evidence suggests that statins may also act as chemoprotective agents against various types of cancers (Wali and Sylvester, 2007). For example, several studies have shown that statins suppress the growth and/or induce apoptosis of breast adenocarcenoma cells *in vitro* (Campbell et al., 2006; Kotamraju et al., 2007; Koyuturk et al., 2007). The antitumor effects of statins in breast carcinoma cells have been associated with their activity as potent inhibitors of 3-hydroxy-3-methylglutaryl-coenzyme A (HMGCoA) reductase, an enzyme catalyzing the conversion of HMGCoA to mevalonate, the rate limiting step in cholesterol biosynthesis (Wali and Sylvester, 2007). Statin-induced inhibition of mevalonate synthesis also reduces the synthesis of downstream non-sterol products such as farnesyl pyrophosphate, which are essential for the isoprenylation of various cellular proteins (Wali et al., 2009; Wali and Sylvester, 2007). These proteins are vital for cellular growth, and isoprenylation is needed for their activation, localization, and function (Goldstein and Brown, 1990). Therefore, early investigations showed that HMGCoA inhibitor blockade of mevalonate synthesis induced cell cycle arrest *in vitro* (Campbell et al., 2006; Graaf et al., 2004; Kaneko et al., 1978; Maltese et al., 1985) and inhibited tumor growth *in vivo* (McIntyre et al., 2000a; Shibata et al., 2003; Thibault et al., 1996). Nevertheless, while the growth inhibitory and pro-apoptotic properties of statins may have important clinical implications, both in the prevention and treatment of certain malignancies (Sassano and Platanias, 2008), the clinical application of statin use has been limited by their high-dose toxicity that can result in rhabdomyolysis and even death (Thibault et al., 1996).

As with statins, vitamin E extract of palm oil, which is commonly referred to as tocotrienol-rich-fraction or TRF, was shown to reduce HMGCoA reductase activity by causing post-transcriptional down-regulation of the enzyme (McIntyre et al., 2000a,b). TRF (Fig. 1) is an oily mixture of tocopherols and tocotrienols, in which tocotrienols constitutes 70–90% of the blend (McIntyre et al., 2000a). Both tocopherols and tocotrienols have similar chemical structure characterized by a phytyl side chain attached to a chromane ring. The difference between the isoforms of tocopherols and tocotrienols, however, lays in the degree of methylation of their chromane ring and the saturation of the phytyl chain (McIntyre et al., 2000b). Although chemically very similar, tocotrienols were shown to possess significantly greater antiproliferative and apoptotic activity than tocopherols in breast cancer cells, using treatment doses that have little or no effect on normal cell growth or viability (McIntyre et al., 2000a,b; Samant and Sylvester, 2006; Shah et al., 2003; Shah and Sylvester, 2004).

* Corresponding author at: Department of Basic Pharmaceutical Sciences, College of Pharmacy, University of Louisiana at Monroe, 1800 Bienville Drive, Monroe, LA 71201, United States. Tel.: +1 318 342 1726; fax: +1 318 342 1737.
E-mail address: nazzal@ulm.edu (S. Nazzal).

0378-5173/$ – see front matter © 2010 Elsevier B.V. All rights reserved.
doi:10.1016/j.ijpharm.2010.01.018

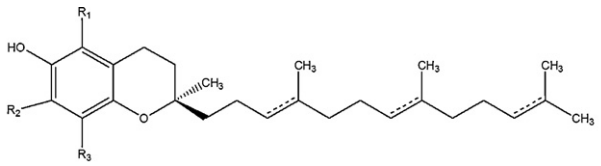

Compound	R_1	R_2	R_3	Phytyl chain
α-tocopherol	CH_3	CH_3	CH_3	Saturated
γ-tocopherol	H	CH_3	CH_3	Saturated
δ-tocopherol	H	H	CH_3	Saturated
α-tocotrienol	CH_3	CH_3	CH_3	Unsaturated
γ-tocotrienol	H	CH_3	CH_3	Unsaturated
δ-tocotrienol	H	H	CH_3	Unsaturated

Fig. 1. Generalized chemical structure of vitamin E.

Since the mechanism of action by which tocotrienols and statins suppress HMGCoA reductase activity is different, a combined low dose treatment with gamma tocotrienol and statins was shown to synergistically inhibit the growth of highly malignant +SA mammary epithelial cells in culture (Wali and Sylvester, 2007). Specifically, Wali and Sylvester (2007) demonstrated that treatment with 0.25 μM simvastatin (Fig. 2) or 2.0 μM gamma tocotrienol alone had no effect, while combined treatment of simvastatin with gamma tocotrienol significantly inhibited the proliferation of malignant +SA mammary epithelial cells. Combining low dose statin and tocotrienol was shown to induce mammary tumor cell cycle arrest at Gap phase 1 (G1), resulting from an increase in p27 expression, and a corresponding decrease in cyclin D1, CDK2, and hypophosphorylation of Rb protein (Wali et al., 2009). These findings suggested that combined treatment of statins with tocotrienols may provide significant health benefits in the prevention and/or treatment of breast cancer, while avoiding myotoxicity associated with high dose statin monotherapy (Wali et al., 2009).

A barrier to successful cancer therapy via a combined TRF/simvastatin treatment, however, lays in the challenge of delivering the required therapeutic concentration of the drugs to the tumor cells while minimizing non-specific toxicity resulting from their systemic administration This could be circumvented by passively targeting simvastatin and tocotrienols coencapsulated in the form of lipid nanoparticles to tumor cells. Lipid nanoparticles

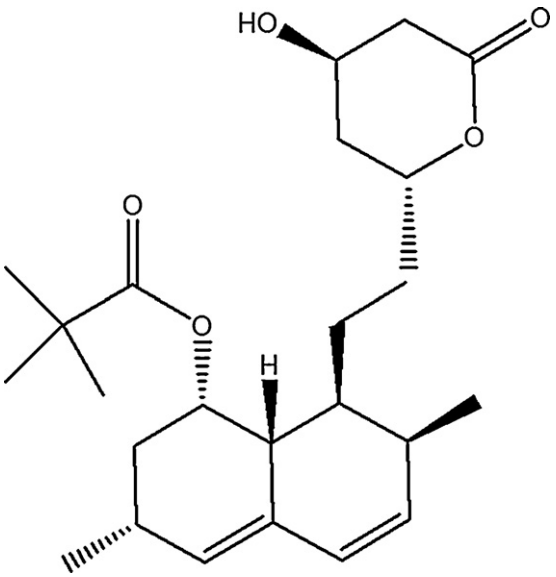

Fig. 2. Chemical structure of simvastatin (SIM).

along with the entrapped drugs readily penetrate tumors due to the tumors' discontinuous and leaky microvasculature (Hobbs et al., 1998; Pasqualini et al., 2002). Also, poor lymphatic drainage of tumors may result in slower clearance of the nanoparticles and their subsequent accumulation in tumor cells (Dong et al., 2009). These structural features of many solid tumors are commonly referred to as the enhanced vascular permeability and retention (EPR) effect. The selective extravasation and retention of the nanoparticles in tumors is therefore expected to potentiate the effect of tocotrienol while minimizing the side effects associated with the systemic administration of simvastatin.

The aim of this work was to examine whether the *in vitro* antiproliferative effects of SIM and TRF are retained when they are combined and coencapsulated within the cores of lipid nanoparticles. Lipid nanoparticles such as nanostructure lipid carriers (NLCs) and solid lipid nanoparticles (SLNs) are aqueous colloidal dispersions with a size in the range of 50–1000 nm. The matrix of SLNs is composed of biodegradable and biocompatible solid lipids (Castelli et al., 2005). Unlike SLNs, however, the cores of the NLCs are composed of blends of lipids in which liquid low melting-point lipids, such as TRF, are entrapped in the form of oily nanocompartments within a solid matrix (Jenning et al., 2000; Muller et al., 2002). Due to their lipophilic matrix, SLNs and NLCs are ideal for the administration of chemotherapeutic agents (Ma et al., 2009) and lipophilic drugs, such as simvastatin and TRF. The specific objectives of this study were therefore to (1) assess the physicochemical properties of the simvastatin–TRF nanoparticles, such as particle size, surface morphology, drug entrapment efficiency, *in vitro* drug release, and stability and (2) evaluate the cellular antiproliferative effect of the simvastatin–TRF nanoparticles against the highly malignant neoplastic +SA mammary epithelial cells.

2. Materials and methods

2.1. Materials

Compritol® 888 ATO (glyceryl behenate, melting point: 71–74 °C), which is a mixture of ~15% mono-, 50% di- and 35% triglycerides of behenic acid, was provided by Gattefossé (Saint-Priest, Cedex, France); methanol HPLC grade, (±)-α-tocopherol (αT); methylthiazolyldiphenyl tetrazolium bromide (MTT), bovine serum albumin (BSA), and other chemicals for cell culture experiments were purchased from Sigma Chemical Company (St. Louis, MO, USA); Lutrol® F 68 NF (poloxamer 188) was obtained from BASF (Florham Park, NJ); simvastatin (SIM) was purchased from Haorui Pharma-Chem Inc. (Edison, NJ); tocotrienol-rich-fraction of palm oil (TRF), which contains 9.8% α-tocopherol, 27.9% α-tocotrienol, 41.4% γ-tocotrienol, 19.2% δ-tocotrienol was a gift from Davos Life Science PTE LTD. (Singapore); water was obtained from NanoPure purification system. All chemicals were used as supplied without further modification.

2.2. Preparation of the lipid nanoparticles

Nanoparticles were prepared by the o/w microemulsion technique using high-shear homogenization as described by Ahlin et al. (1998) with slight modification. Briefly, Compritol® 888 ATO (COMP) alone or in combination with SIM, TRF (or αT), were allowed to melt at 80 °C, meanwhile in a separate vial, Lutrol® F68 was dissolved in purified water and heated to 80 °C. The hot surfactant solution was then added to the molten lipid under high-shear homogenization at 20,000 rpm using IKA® Ultra-Turrax T10 homogenizes fitted with a rotor-stator type S10N-8G (IKA® Works Inc., NC, USA). After 5 min, the o/w microemulsion was sonicated for 10 min using an ultrasonic homogenizer at 60% pulsar rate

Table 1
Composition, intensity weighed Z-average particle diameter (Z-ave), and zeta potential (ZP) of unloaded SLNs and TRF or αT NLCs with or without SIM. Each point represents mean ± SD.

Formulation	COMP (% w/v)	αT (mM)	TRF (mM)	SIM (mM)	Polox. 188 (% w/v)	Z-ave (nm)	PI	ZP (mV)
Unloaded SLN[a]	0.50	0	0	0	0.25	151.7 ± 1.2	0.28 ± 0.00	−21.7 ± 0.8
SIM-TRF NLC[b]	0.25	0	5	1	0.25	107.5 ± 0.73	0.29 ± 0.01	−13.4 ± 0.4
SIM-αT NLC[c]	0.25	5	0	1	0.25	106.8 ± 2.54	0.253 ± 0.01	−9.0 ± 0.8
TRF-NLC[d]	0.25	0	5	0	0.25	100.3 ± 0.91	0.233 ± 0.01	−13.5 ± 0.4
αT-NLCs[e]	0.25	5	0	0	0.25	101.2 ± 1.27	0.203 ± 0.02	−10.5 ± 1.2

[a] Unloaded SLNs, blank solid lipid nanoparticles made from Compritol 888 ATO (COMP) only as a lipid phase.
[b] SIM-TRF-COMP NLCs, nanostructure lipid carriers with simvastatin and tocotrienol rich fraction (TRF).
[c] SIM-αT-COMP NLCs, nanostructure lipid carriers with simvastatin and α-tocopherol (αT).
[d] TRF-NLCs, nanostructure lipid carriers with TRF.
[e] αT-NLCs, nanostructure lipid carriers with αT.

(Model 150VT, Biologics, Inc., Manassas, VA). After homogenization, nanoparticles were formed by congealing the sonicated dispersions overnight at 4 °C. The concentrations of the lipid phase, including TRF (or αT), and the emulsifier in the dispersions were 0.50% and 0.25% (w/v), respectively. The amount of SIM and TRF (or αT) added to the lipid phase was adjusted so as to obtain dispersions that contain 1 mM of SIM and 5 mM of either TRF or αT. The compositions of the nanoparticles that were evaluated in this study are listed in Table 1. For the DSC and PXRD studies either binary blends of TRF (or αT) with COMP or ternary blends of SIM, TRF (or αT), and COMP were evaluated. The binary blends were prepared by mixing the TRF (or αT) with molten COMP to 85 °C. Ternary blends were prepared by dissolving SIM in the molten COMP/TRF (or αT) blends. Molten blends were allowed to re-congeal at room temperature overnight prior to their analysis.

2.3. Differential scanning calorimetry (DSC) studies

Thermal analysis was performed to examine the physical state of SIM in the nanoparticles. DSC analyses were performed using a 2920 Modulated DSC (TA Instruments-Waters LLC, New Castle, DE). DSC runs were performed on fresh samples as well as samples stored at controlled room temperature for 6 months. These samples include (A) COMP/TRF (or αT) binary blend (at ratio 1:1 by weight), (B) physical mixture of SIM, TRF (or αT), and COMP (at ratio 0.2:1:1 by weight), and (C) SIM-TRF (or αT)-COMP ternary blend (at ratio 0.2:1:1 by weight. Samples (2–10 mg) were hermetically sealed in aluminum pans were heated from 20 °C to 170 °C at a rate of 10 °C/min. Melting endotherms were estimated from the generated data using Universal analysis 2000 version 4.2E software (TA Instruments-Waters LLC, New Castle, DE).

2.4. Powder X-ray diffraction (PXRD) measurements

PXRD was performed to determine the crystallinity of fresh samples as well as samples stored at controlled room temperature for 6 months. These samples include (A) COMP/TRF (or αT) binary blend (at ratio 1:1 by weight), (B) physical mixture of SIM, TRF (or αT), and COMP (at ratio 0.2:1:1 by weight), and (C) SIM-TRF (or αT)-COMP ternary blend (at ratio 0.2:1:1 by weight). X-ray diffraction patterns were obtained by wide-angle X-ray scattering (WARS, $2\tau = 5–50^{\circ}$, step size = 0.5) using a Philips PW 1830 X-ray generator (Philips, Amedo, Netherlands) fitted with a copper anode tube (Cu Kα radiation, λ = 1.5418 nm) and a Goniometer PW 18120 detector. Data of the scattered radiation were recorded at an anode voltage of 40 kV and a current of 35 mA.

2.5. Determination of SIM-NPs entrapment efficiency

The entrapment efficiency (EE) of the SIM NLCs was determined by measuring the concentration of the free unloaded SIM in the aqueous phase of the NLC dispersions. Approximately 1.0 mL of the dispersion was placed in the inner chamber of an Ultracel-30K Millipore filters assembly having a molecular weight cutoff (MWCO) of 30,000 Da (Millipore Corporation, Billerica, MA). The assembly was then centrifuged at 5000 rpm (approximately 3000 × *g*) for 15 min at 5 °C using Eppendorf® 580R centrifuge (Hamburg, Germany). The NLCs along with the encapsulated SIM remained in the inner chamber whereas the aqueous dispersion medium containing the free SIM moved to the sample recovery chamber through the filter membrane. After separation, the amount of the free SIM in the dispersion medium was estimated by HPLC. SIM entrapment efficiency and SIM loading were subsequently calculated from the following equation:

$$\text{Entrapment efficiency (\%)} = \frac{\text{Amount of SIM entrapped in NLCs}}{\text{Theoretical total amount of SIM added to NLCs}} \times 100$$

$$\text{SIM loading (\%)} = \frac{\text{Amount of SIM entrapped in NLCs}}{\text{Amount of solid lipid + amount of SIM}} \times 100$$

Amount of SIM entrapped in NLCs was calculated by subtracting the amount of free SIM from the theoretical amount of SIM added to NLCs.

2.6. HPLC analysis

The concentration of SIM in the nanoparticle dispersions was determined by a reversed-phase HPLC method, which was previously described in detail (Ali and Nazzal, 2009). This method was validated for TRF and SIM over a concentration range of 20–80 μg/mL and 1–10 μg/mL, respectively. Briefly, the solution collected from the recovery chamber (as discussed in Section 2.5 above) was injected into a C_{18} (4.6 mm × 100 mm) Onyx® monolithic analytical column (Phenomenex®, Inc., Torrance, CA) supported by a SpectraSystem HPLC (Thermo Electron Corporation, San Jose, CA) equipped with a UV3000 UV/vis variable wavelength detector. The detection of SIM was carried out at λ_{max} = 238 using a 15% (v/v) water in methanol solution as the mobile phase, which was allowed to run at a flow rate of 1 mL/min. Data acquisition was performed using a chromatography software ChromQuest™ version 4.2 (Thermo Electron Corporation, San Jose, CA).

2.7. Determination of particle size (Z-ave), polydispersity index (PI), and zeta potential (ZP)

The intensity-weighed mean particle size, population distribution (polydispersity index), and zeta potential of the nanoparticles were measured by photon correlation spectroscopy (PCS) at 25 °C and 90° fixed angle using Nicomp™ 380 ZLS zeta potential and submicron particle size analyzer (PSS Inc., Santa Barbara, CA). When needed, samples were diluted with deionized water, which was

previously filtered through a 0.2 μm filter membrane. Analyses were performed in triplicates unless otherwise specified.

2.8. Cryo-scanning electron microscopy (cryo-SEM)

The size and morphology of the nanoparticles were observed using a Type FP 2012/13 Quanta 200 scanning electron microscope (FEI, Netherlands) fitted with a Gatan/Alto 2100 Cryotrans System (Gatan Instruments, Oxon, UK). To minimize potential morphological changes during the SEM drying process, NLCs were cryotransferred with liquid nitrogen prior to analysis. This was achieved by first cooling and maintaining the NLC samples for at least 1 min at −170 °C by liquid nitrogen in the Cryotrans System. Then the samples were freeze-fractured with a cryo-honing device. The temperature of the freeze-fractured specimen was then raised to −80 °C to allow controlled sublimation of the water. This etching process was arrested by rapidly lowering the temperature to −170 °C. Finally, the specimens were coated with gold and examined by SEM.

2.9. In vitro drug release

The release of SIM from either SIM-TRF NLCs or SIM-αT NLCs was measured at 37 °C under sink conditions. One milliliter of either NLC dispersion (equivalent to 0.4 mg SIM) was suspended in 9.0 mL phosphate buffer saline (PBS, pH 7.4) containing 30% ethanol. Aliquots of the dissolution medium were withdrawn at different time intervals and replaced with fresh dissolution medium to maintain a constant volume. Collected samples were centrifuged using Ultracel-30K Millipore filters at 5000 rpm (approximately 3000 × *g*) for 15 min at 5 °C using Eppendorf® 580R centrifuge (Hamburg, Germany) to separate the nanoparticles from the free SIM. The NLCs along with the encapsulated SIM remained in the inner chamber whereas SIM released into the dissolution medium was recovered in the outer chamber. The concentration of the released SIM was determined by HPLC as described above. All experiments were carried out in triplicates. Results were expressed as means ± standard deviation.

2.10. Stability study

Nanoparticle dispersions were stored protected from light at controlled room temperature for 6 months. At different time intervals the particle size (Z-ave), polydispersity index (PI), entrapment efficiency (EE), and zeta potential (ZP) of the dispersions, were measured as described above.

2.11. In vitro antiproliferation studies

2.11.1. Cell line and culture conditions

Experiments conducted in this present study represent a logical contribution of previous studies that have extensively characterized the antiproliferative and apoptotic effects of tocotrienols in the highly malignant +SA mammary epithelial cell line (McIntyre et al., 2000a,b; Samant and Sylvester, 2006; Shah et al., 2003; Shah and Sylvester, 2004; Wali et al., 2009; Wali and Sylvester, 2007). This cell line was derived from an adenocarcinoma that developed spontaneously in a BALB/c female mouse (Danielson et al., 1980). The +SA cell line is characterized as being highly malignant, estrogen-independent, and displays anchorage-independent growth when cultured in soft agarose gels. When +SA cells are injected back into the mammary gland fat pad of syngeneic female mice, they form rapidly growing anaplastic adenocarcinomas that are highly invasive and metastasize to the lung (Danielson et al., 1980). Cell culture and the experimental procedures used in this present study have been previously described in detail (McIntyre et al., 2000a). Briefly, cells were grown and maintained in serum-free Dulbecco's modified Eagle's medium (DMEM)/F12 control media containing 5 mg/mL bovine serum albumin (BSA), 10 μg/mL transferrin, 100 μg/mL soybean trypsin inhibitor, and 100 U/mL penicillin and 100 μg/mL streptomycin, 10 μg/mL insulin, and 10 ng/mL EGF as a mitogen. Cells were maintained at 37 °C in a humidified atmosphere of 95% air and 5% CO_2.

2.11.2. Measurement of viable cell number

Viable cell number was determined using the 3-(4,5-dimethylthiazol-2yl)-2,5-diphenyl tetrazolium bromide (MTT) colorimetric assay as previously described (McIntyre et al., 2000a). Briefly, at the end of the treatment period, media in all treatment groups were removed and replaced with fresh control media containing 0.42 mg/mL MTT, and the cells were returned to the incubator for a period of 4 h. At the end of the incubation period, media was removed, the MTT crystals were dissolved in 1 mL of isopropanol, and the optical density of each sample was read at 570 nm on a microplate reader (SpectraCount, Packard BioScience Company, Meriden, CT). Cell number was calculated against a standard curve prepared by plating known concentrations of cells, as determined by the hemocytometer, at the start of each experiment.

2.11.3. Experimental treatments

For all experiments, freshly prepared nanoparticle dispersions were filtered through either 0.22 or 0.45 μm sterile syringe filters. These dispersions were then added to the culture media at various concentrations to prepare treatment media supplemented with TRF or αT NLCs with or without SIM. Each time, the treatment media was prepared freshly just before the treatment. The sterile stock formulations were stored at 4 °C throughout the duration of the experiment.

2.11.4. Treatments and statistical analysis

+SA cells were initially plated at a density of 5×10^4 cells/well (6 wells/group) in serum-free defined control media in 24-well culture plates and allowed to adhere overnight. The following day, cells were divided into different treatment groups and media was removed and replaced with fresh control or treatment media, and then returned to the incubator. Cells in their respective treatment groups were fed fresh media every other day throughout experimentation. IC_{50} values (dose resulting in 50% cell growth inhibition) for the TRF or αT NLCs with or without SIM were determined by non-linear regression curve fit analysis using GraphPad Prism 5 (GraphPad Software, La Jolla, CA). Differences among the various treatment groups in cell growth and viability studies were determined by analysis of variance (ANOVA) followed by Duncan's *t*-test. A difference of $p < 0.05$ was considered to be significant as compared to vehicle-treated controls.

3. Results and discussion

3.1. Preliminary solubility, DSC, PXRD studies

In order to incorporate a drug into SLNs it should possess a sufficiently high solubility in the solid lipid. Therefore, prior to SLN preparation, a preliminary study was performed to determine if SIM could be dissolved in COMP. This was done by dissolving various amounts of SIM in molten COMP. After cooling and re-solidification, however, SIM crystals were readily seen when the COMP/SIM blends were inspected by polarized light microscopy. As a consequence, it was prudent to develop NLCs in which a liquid oil is added to the solid lipid in order to enhance SIM payload in the nanoparticles. This was achieved by substituting a portion of the lipid phase (i.e., COMP) with either TRF (or αT). TRF and αT introduced imperfections to the ordered crystalline structure of COMP

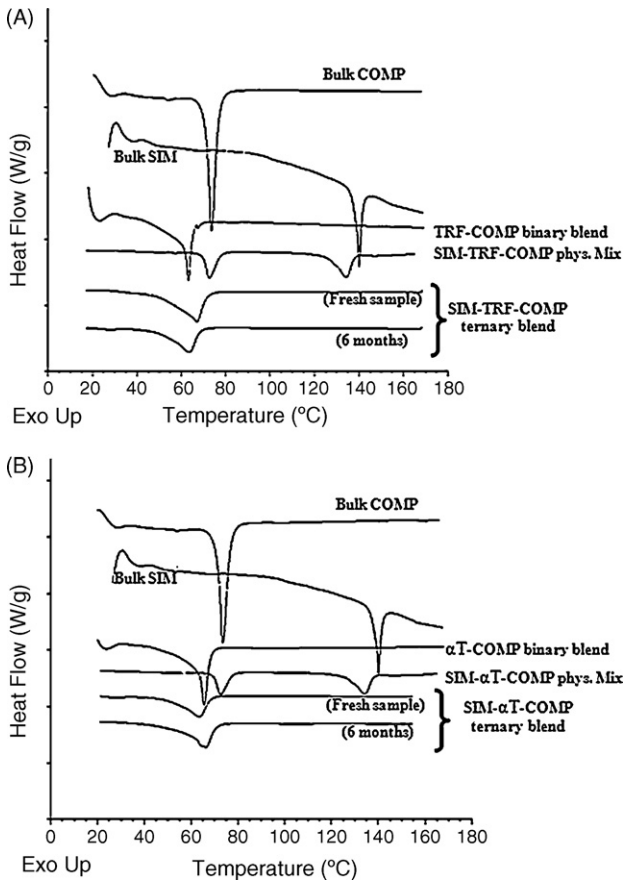

Fig. 3. DSC profiles of TRF based (A) and αT based (B) blends showing the endotherms of bulk Compritol 888 ATO (COMP), bulk simvastatin (SIM), COMP/TRF (or αT) binary blend (at ratio 1:1 by weight), physical mixture of SIM-TRF (or αT) SIM-COMP (at ratio 0.2:1:1 by weight), and SIM-TRF (or αT) SIM-COMP ternary blend (at ratio 0.2:1:1 by weight), when freshly prepared and after 6 months of storage; curves were displaced along the ordinate for better visualization.

(as discussed below) and were therefore expected to facilitate SIM incorporation into the nanoparticles.

Various formulations were screened by substituting 10–50% (by weight) of COMP with either TRF or αT. Complete dissolution was observed when blends with 50% TRF (or αT) were used. This was confirmed when the blends were inspected by polarized light microscopy. Absence of visible crystals in the formulations in which 50% of COMP was substituted with TRF or αT indicated that SIM was present as a solid solution and was molecularly dispersed in the lipid matrix. DSC and PXRD studies were performed to further confirm the dissolution of SIM in the COMP/TRF (or αT) blends.

DSC is an established technique that has been used to characterize solid dispersions, and to evaluate drug–lipid interactions and the degree of crystallization and polymorphism of drugs (Bunjes and Unruh, 2007). Therefore, DSC was used to study the physical state of SIM in TRF (or αT) blends with solid lipids as a precursor to understanding the physical behavior of SLNs. The first step in this investigation was to characterize TRF-COMP and αT-COMP binary blends. As described in Section 2, binary blends were prepared by mixing either TRF or αT with the molten lipid (COMP) at 85 °C. Once cooled, the melting point of the solid mixtures was measured by DSC. The thermograms of TRF-COMP and αT-COMP binary blends (Fig. 3) revealed endothermic peaks at approximately 63 °C and 65 °C, respectively, which were lower than the melting point of the bulk COMP (~73 °C). Lower melting points implied that an interaction between COMP and either TRF (or αT) resulted in a decrease in the crystallinity of the COMP/TRF (or αT) lipid matrix.

In the next step, DSC complemented with PXRD measurements was used to investigate the physical state of SIM in either TRF-COMP or αT-COMP blends. The DSC thermograms corresponding to the physical mixtures of SIM, COMP, and either TRF or αT were compared to those of SIM-TRF-COMP or SIM-αT-COMP ternary blends. The ternary blends were prepared at the same proportions as in SLNs by solubilizing SIM in the molten TRF-COMP or αT-COMP blends. As shown in the DSC thermograms (Fig. 3), the physical mixture of either SIM-TRF-COMP or SIM-αT-COMP, showed two distinct endothermic peaks at approximately 73 °C, which corresponded to the melting point of COMP, and 133 °C (or 140 °C in the case of αT), which corresponded to the melting point of SIM. The presence of two distinctive endotherms indicated that both SIM and COMP were in crystalline state and that an interaction did not exist between COMP and either TRF or αT. In contrast, DSC profiles of the ternary blends revealed a single broad endotherm at 60 °C and 71 °C, for SIM-TRF-COMP and SIM-αT-COMP, respectively, which suggested the presence of SIM as a molecular dispersion in the partially crystalline COMP. No change was observed in the thermal plots of the ternary blends after 6 months of storage (Fig. 3).

To confirm the data generated by DSC and polarized light microscopy, samples were analyzed by wide-angle powder X-ray diffraction (PXRD). The X-ray diffraction pattern for bulk SIM revealed major peaks at $2\theta = 9.25$, 16.75, 17.25, 18.75, 22.75, 25.25, 28.25, and 31.75 (Fig. 4). The intensity of the peaks decreased when SIM was physically mixed with either TRF (or αT), and COMP, which could be attributed to lower SIM loading. Nonetheless, the apparent peaks at $2\theta = 16.75$, 17.25, and 18.75 in the physical mixture indicate the presence of SIM in crystalline form. These peaks disappeared from the diffraction pattern of the solidified ternary blends. These blends were prepared by solubilizing SIM in the molten TRF (or αT) COMP blends in a process that simulated NLCs production. The peak at $2\theta = 20.75$ accompanied with a small shoulder of low intensity at $2\theta = 21.25$ correspond to COMP β′-modification (Souto et al., 2006). These results confirmed the existence of SIM as a molecular dispersion in the TRF-COMP or αT-COMP blends. As with DSC, no changes in the crystallinity of the ternary blends were seen after six month of storage (Fig. 4), which validated the observed long term stability and high entrapment efficiency of SIM in the nanoparticles as discussed in Section 3.2 below.

3.2. Particle size (Z-ave), zeta potential (ZP), and entrapment efficiency (EE)

Nanoparticles were prepared from their microemulsion precursors by high-shear homogenization followed by ultrasonication. The compositions of the nanoparticles, their Z-ave diameters, and polydispersity indexes (PI) are listed in Table 1. The Z-ave of the SLNs was 152 nm. The size of the nanoparticles, however, decreased significantly when 50% of COMP was substituted with TRF (or αT). For instance, the Z-ave for TRF based NLCs was ~100 nm whereas the Z-ave of unloaded SLNs was ~152 nm. Lower particle size could be attributed to the efficient packing of the disrupted crystalline structure of COMP when blended with TRF (or αT). These data also suggested that SLNs can encapsulate liquid oils up to 50% by weight without compromising the size of the nanoparticles. The entrapment of SIM into NLCs did not change the size of the nanoparticles. SIM NPs had a particle sizes ~100 nm, which should be ideal for future *in vivo* administration. Nonetheless, the size of the nanoparticles may vary with factors such as the difference in temperature between the warm microemulsion and the refrigerator during the cooling process and the composition of each formulation. These factors were maintained constant in this study. Variations to these factors will be considered in future work.

Polydispersity index (PI) is considered an indicator of particle distribution. All nanoparticle dispersions had PI values in the range

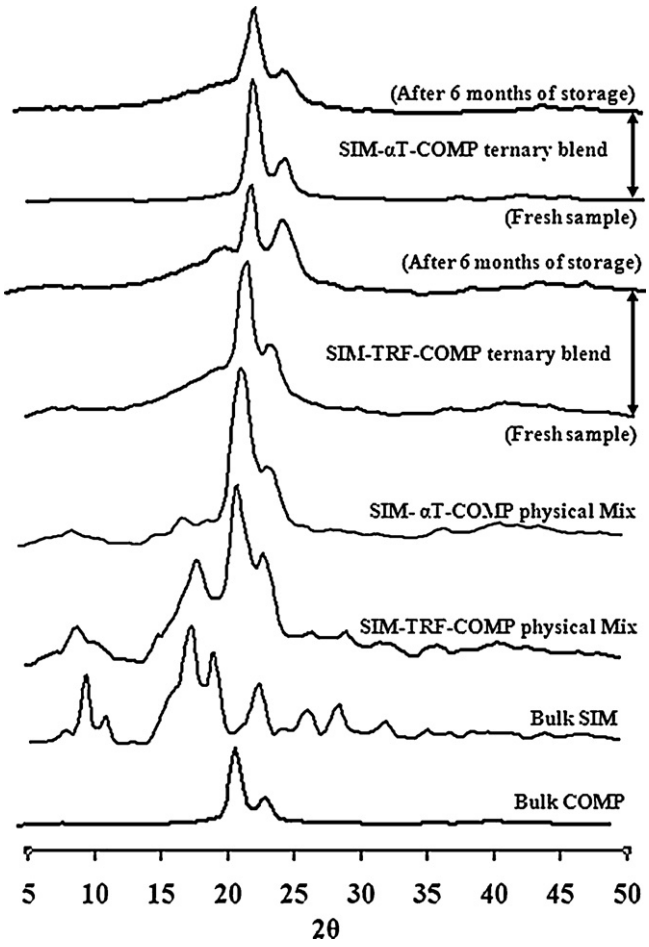

Fig. 4. Powder X-ray diffraction patterns. From bottom to top, bulk simvastatin (SIM), SIM in physical mixture with TRF and COMP (0.2:1:1 by weight), SIM in physical mixture with αT and COMP (0.2:1:1 by weight), SIM blend with TRF and COMP (0.2:1:1 by weight) freshly prepared and after six month of storage at controlled room temperature, SIM blend with αT and COMP (0.2:1:1 by weight) freshly prepared and after six months of storage. Curves were displaced along the ordinate for better visualization.

from 0.20 to 0.29 (Table 1), which indicated that the nanoparticles prepared in this study were mono-disperse. TRF or αT incorporation into SLNs, however, significantly decreased PI, which reflected their positive impact on dispersion uniformity.

With regard to the stability of SLNs and NLCs, it was reported that ZP values below −30 mV impart sufficient electrostatic repulsion between the nanoparticles, which favor improved physical stability (Freitas and Muller, 1998). The use of steric stabilizers was also shown to produce stable formulations (Heurtault et al., 2003). In our study, all nanoparticles had ZP values in the range from −9.0 to −21.0 mV. While the ZP values were less than |−30 mV|, the Z-ave did not significantly change over six months of storage at room temperature (data shown in Section 3.5 below). The long-term stability of the nanoparticles could be attributed to poloxamer 188. It was reported that while poloxamer 188, a non-ionic surfactant, decreases the electrostatic repulsion between the particles, it sterically stabilizes the nanoparticles by forming a coat around their surface (Schwarz et al., 1994). Furthermore, COMP was chosen as the SLN matrix forming material because it was shown in earlier screening studies to produce stable nanoparticles.

After the preparation of the nanoparticles, there was no evidence of separation of either liquid oils or SIM. To confirm SIM retention within the NLCs, entrapment efficiency study was preformed. The EE% of SIM in SIM-TRF NLCs and SIM-αT NLCs was

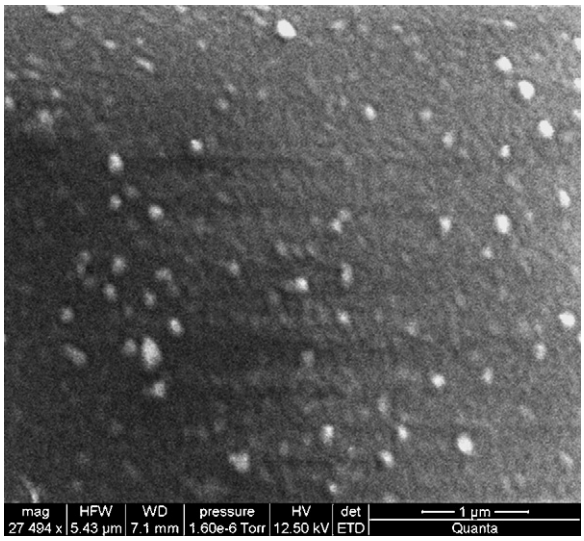

Fig. 5. Representative Cryo-SEM image of SIM-TRF NLCs. These NLCs were composed of SIM (1 mM), TRF (5 mM), poloxamer 188 (0.125%, w/v), and Compritol 888 ATO (0.25%, w/v).

99.9 ± 1.3 and 99.9 ± 0.8, respectively. High entrapment efficiency of SIM in the NLCs could be attributed to the presence of the liquid nanocompartments formed by TRF (or αT), which were entrapped within the solid matrix of the NLCs. In essence, NLCs served as nanoreservoir drug delivery systems for SIM. These results confirmed earlier DSC and PXRD data with regard to SIM dissolution in the COMP/TRF (or αT) blends.

3.3. Cryo-scanning electron microscopy (cryo-SEM)

Cryo-SEM images were collected to investigate the morphology of the SIM-NLCs. As shown in the representative image of SIM-TRF NLCs (Fig. 5), nanoparticle had spherical or ellipsoidal shapes. No SIM nanocrystals were visible. The size of the nanoparticles as

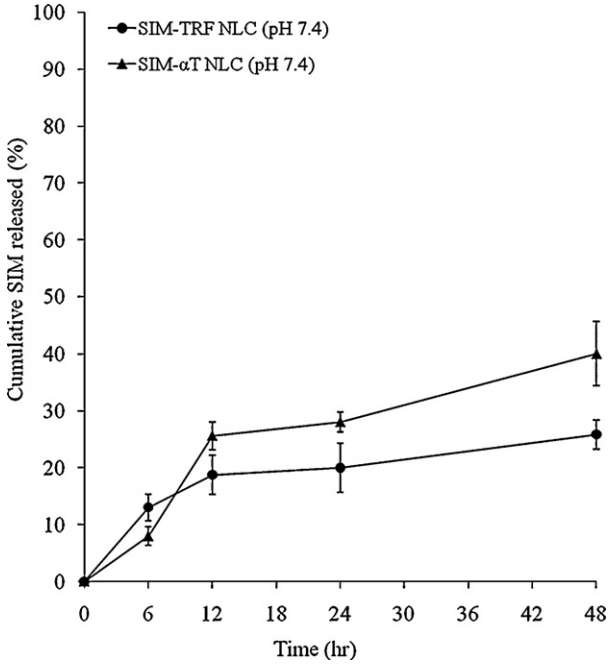

Fig. 6. *In vitro* release profiles of SIM-NLCs formulations at 37 °C in phosphate buffer saline containing 30% ethanol at pH 7.4. Data are represented as the mean ± SD ($n = 3$).

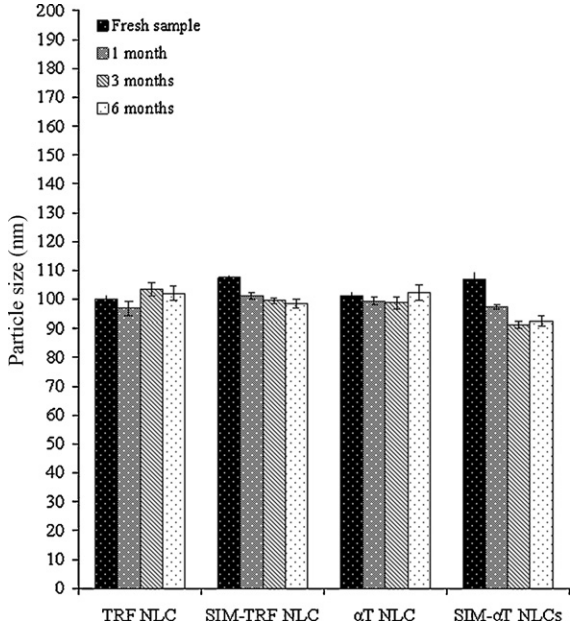

Fig. 7. Long-term stability of NLC formulations stored at 25 °C. Formulations were monitored for their Z-ave particle diameters over six months. All samples showed PI < 0.35. All data are represented as the mean ± SD ($n = 3$).

determined from the Cryo-SEM images correlated well with the particle size data that were reported in Table 1.

3.4. In vitro drug release

The release of SIM from the NLC formulations was measured *in vitro* over 48 h. Due to the low water solubility of SIM, 30% of ethanol in PBS buffer (pH 7.4) was used as the dissolution medium. Ethanol was added to the medium in order to solubbilize the released SIM and to maintain sink conditions. The release profile of SIM from the NLCs at pH 7.4 is shown in Fig. 6. As shown, a biphasic SIM release pattern was observed. A burst period characterized by a fast SIM release was evident in the first 10 h followed by a slower and controlled release until the end of the experiments. Similar release pattern was reported for other SLN formulations, whereby an initial fast release is followed by a slow and incomplete release of drug (Wong et al., 2007).

The cumulative percentage of SIM released ranged from 25% to 40% over the 48 h test period. The cumulative amount of SIM released from αT based NLCs was higher than the corresponding cumulative amount released from the TRF based NLCs. A significantly lower amount of SIM was released from the SIM-TRF-COMP NLCs, with only 25% released after 48 h at pH 7.4. These results indicated that SIM, which was incorporated into TRF based NLCs, was likely to remain associated with the nanoparticles. While only a fraction of the drug was released into the media, the cytoxocity of the formulations may not be affected. It has been shown that SLN formulations in which only a fraction of the drug is released are more cytotoxic than the free drug indicating that the cytotoxic compounds that remain associated with the nanoparticles are effective (Wong et al., 2007). The difference in release between the TRF and αT based NLCs could be attributed to the higher viscosity of TRF, which may retard the diffusion of SIM from the nanoparticles as predicted by the Stokes–Einstein's law (Teeranachaideekul et al., 2007). Furthermore, the slow and sustained release of SIM after the initial burst period indicated that SIM was likely not present at or near the surface of the nanoparticles but instead within the cores of the NLCs as ideally predicted by the enhanced solvation ability of the nanocompartmental domains formed by either TRF or αT.

Table 2
IC_{50} values for the TRF or αT NLCs with or without SIM (mean ± SEM, $n = 6$).

Formulation	IC_{50} (μM)
SIM-TRF NLC	0.52 ± 0.02[a]
SIM-αT NLC	0.76 ± 0.05[b]
TRF-NLC	1.50 ± 0.12[a]
αT-NLC	17.70 ± 0.74[b]

[a] The IC_{50} values for the SIM-TRF NLC and TRF NLC represent the inhibitory concentration of TRF when the antiproliferative effect of the nanoparticles was tested with our without the presence of SIM, respectively.

[b] The IC_{50} values for the SIM-αT NLC and αT NLCs represent the inhibitory concentration of αT when the antiproliferative effect of the nanoparticles was tested with our without the presence of SIM, respectively.

3.5. Long-term stability of NLCs

For the long term stability study, NLC dispersions were stored at room temperature protected from light for 6 months. The Z-ave particle diameter, polydispersity index (PI), zeta potential (ZP) and SIM entrapment efficiency were measured after 1, 3, and 6 months. After 6 months of storage, the Z-ave and ZP of the NLCs did not significantly differ from the freshly prepared samples. Fig. 7 shows the Z-ave of NLCs over 6 months of storage. As shown in the figure, the Z-ave changed from 100 to 102 nm, from 107 to 99 nm, from 101 to 103 nm, and from 106 to 92 nm for TRF-NLCs, SIM-TRF NLCs, αT-NLCs, and SIM-αT NLCs, respectively. PI for all samples was <0.35, indicating narrow distribution and monodispersity (Dong et al., 2009; Lai et al., 2006). These results reflected good long-term stability of the NLC formulations, which was further confirmed by the absence of a distinctive SIM endothermic peak or crystalline pattern when analyzed after 6 months by DSC and PXRD, respectively. To eliminate the possibility of drug expulsion from the nanoparticles during storage, NLC dispersions were visually inspected for signs of phase separation and were analyzed for SIM entrapment efficiency. The percentage of SIM that remained entrapped in the nanoparticles after 6 months of storage only marginally decreased from 99.9 ± 1.3 to 99.2 ± 0.4 and from 99.9 ± 0.8 to 98.9 ± 0.5 for the TRF and αT based NLCs, respectively.

3.6. In vitro anticancer activity

As discussed in the introduction, TRF and SIM were shown to exhibit potent antiproliferative effect against tumor cells when tested *in vitro* (Wali and Sylvester, 2007). This effect was further potentiated when SIM and TRF were combined in the same treatment, reflecting their synergistic activity against tumor cells (Wali et al., 2009). On the other hand, αT did not show antitumor activity at low concentrations (McIntyre et al., 2000b), and therefore it was used as an inert ingredient to solubilize SIM in αT based NLCs. To confirm that the antiproliferation activity of TRF and SIM was retained when they were encapsulated within NLCs, *in vitro* cell viability studies were carried out using neoplastic +SA mammary epithelial cells. The effects of NLCs at various doses of αT and TRF with or without SIM on cell proliferation over a 4 day culture period are shown in Fig. 8. αT based NLCs (Fig. 8A) did not exhibit any significant effect on cellular viability, when compared to the unloaded SLNs (data not shown), indicating absence of cytotoxic effect. Addition of SIM to the αT based NLCs significantly inhibited +SA cell growth in a dose-responsive manner (Fig. 8C). Similarly, when αT was substituted with TRF (Fig. 8B), the cellular viability decreased significantly with TRF treatment from 0.25 to 14 μM. The antiproliferative effect of the NLCs was further potentiated when the cells were treated with SIM/TRF nanoparticles (Fig. 8D).

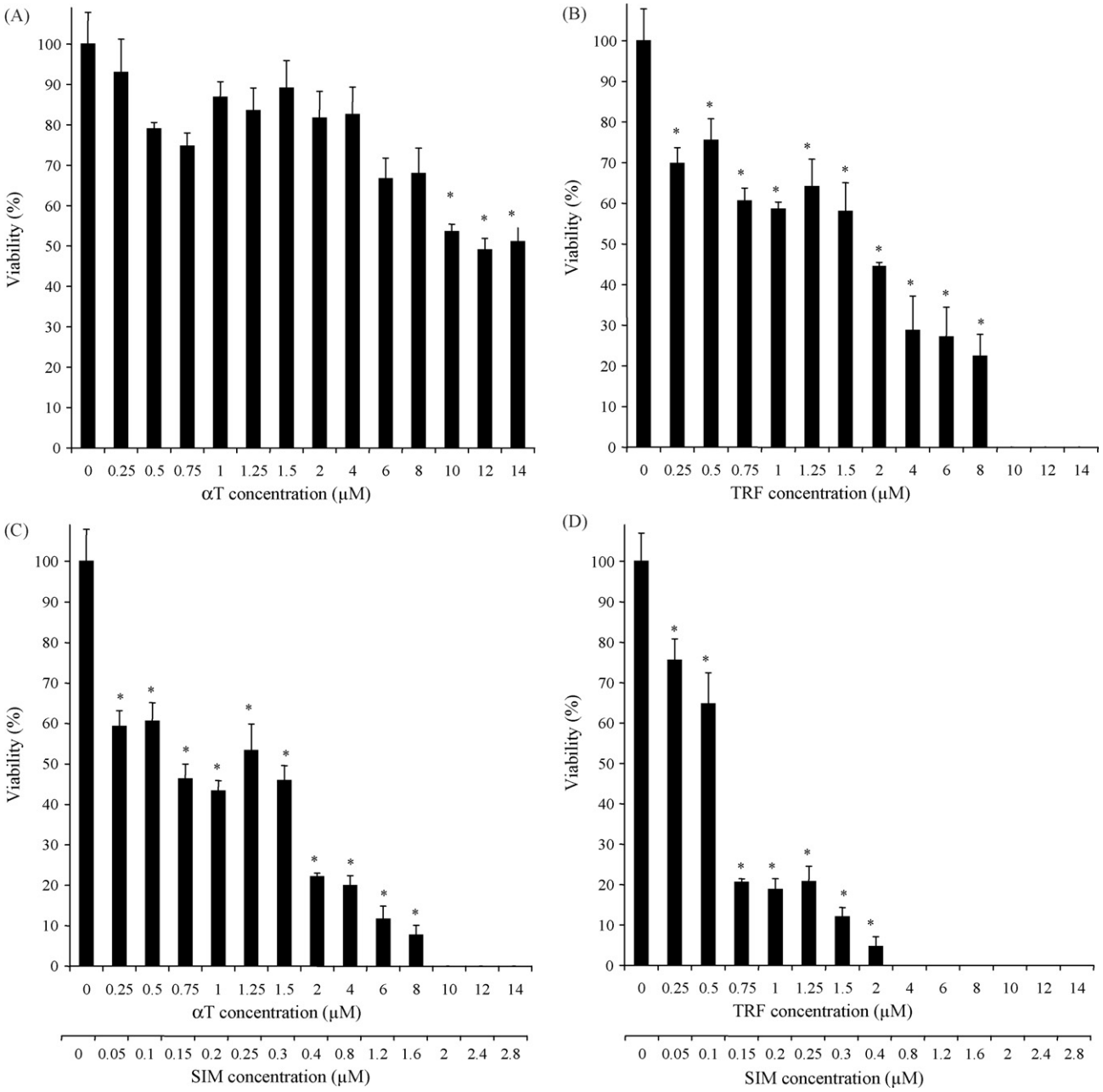

Fig. 8. Anticancer effects of αT NLC (A), TRF NLCs (B), SIM/αT NLCs (C), and SIM/TRF NLCs (D) on neoplastic +SA mammary epithelial cells. Cells were initially plated at a density of 5×10^4 cells/well (6 wells/group) in 24-well plates and exposed to formulation-supplemented media for a 4-day treatment period. Viable cell number was determined using the MTT colorimetric assay. Vertical bars indicate the mean cell count + SEM ($n = 6$). $P < 0.05$ as compared to the vehicle-treated control group.

The antiproliferative effect of the NLCs and the impact of TRF, SIM, and their combination on potentiating the effect of the nanoparticles could be deduced from their 50% growth inhibitory concentration (IC_{50}) values (Table 2). αT based NLCs did not exhibit anticancer activity as evident from their high IC_{50} value (17.7 μM). While treatment with high doses of α-tocopherol may induce anticancer effect, the delivery of such doses is impractical. In comparison, when αT was replaced with TRF, IC_{50} decreased significantly to 1.5 μM, which is less than the reported IC_{50} value (6 μM) when cells were treated with TRF bound to bovine serum albumin (McIntyre et al., 2000b). The lower IC_{50} value of the TRF NLC when compared to the albumin bound TRF might be due to improved internalization of the NLCs by endocytosis into the cells (Serpe et al., 2004; Yuan et al., 2008). Similarly, when SIM was added to the αT based NLCs, at a SIM to αT ratio of 1:5, the IC_{50} decreased to 0.76 μM, reflecting the cytotoxic effect of SIM against +SA mammary epithelial cells. Of most significance, however, was the observed decrease in cell viability and IC_{50} (0.52 μM) when SIM and TRF were coencapsulated into nanoparticles at SIM to TRF ratio of 1:5, which demonstrated the potential therapeutic benefits of a combined SIM and TRF treatment.

4. Conclusion

In this study TRF and SIM were co-encapsulated in lipid nanoparticles for potential use in cancer therapy. The displacement of 50% of COMP in the nanoparticles with TRF (or αT) resulted in morphological changes in the crystalline structure of the solid matrix and produced imperfections that were sufficient to cause a

significant decrease in particle size and a significant increase in SIM payload. The formation of a solid solution in which SIM was molecularly dispersed in the binary blends of TRF (or αT) with COMP was confirmed by DSC and PXRD studies, which showed absence of SIM endothermic or crystalline peaks, respectively. When placed in sink conditions, SIM NLCs exhibited an initial burst release followed by a more gradual release, which was characteristic of this type of nanoparticles. The viability of these nanoparticles for use in cancer therapy was confirmed when the antiproliferative effect of the NLCs was evaluated against neoplastic +SA mammary epithelial cells. Not only was the antiproliferative effect of TRF and SIM retained, their activity was potentiated by their encapsulation into nanoparticles. This could be attributed to enhanced cell binding or NLCs internalization. The exact mechanism of NLCs uptake, however, is the subject of future studies.

Acknowledgements

This work was supported in part by a grant from First Tech International Ltd. The authors would like to acknowledge Dr. John Anderson from the Math and Physics Department for his assistance with the PXRD studies.

References

Ahlin, P., Kristl, J., Šmid-Kober, J., 1998. Optimization of procedure parameters and physical stability of solid lipid nanoparticles in dispersions. Acta Pharm. 48, 257–267.

Ali, H., Nazzal, S., 2009. Development and validation of a reversed-phase HPLC method for the simultaneous analysis of simvastatin and tocotrienols in combined dosage forms. J. Pharm. Biomed. Anal. 49, 950–956.

Bunjes, H., Unruh, T., 2007. Characterization of lipid nanoparticles by differential scanning calorimetry, X-ray and neutron scattering. Adv. Drug Deliv. Rev. 59, 379–402.

Campbell, M.J., Esserman, L.J., Zhou, Y., Shoemaker, M., Lobo, M., Borman, E., Baehner, F., Kumar, A.S., Adduci, K., Marx, C., Petricoin, E.F., Liotta, L.A., Winters, M., Benz, S., Benz, C.C., 2006. Breast cancer growth prevention by statins. Cancer Res. 66, 8707–8714.

Castelli, F., Puglia, C., Sarpietro, M.G., Rizza, L., Bonina, F., 2005. Characterization of indomethacin-loaded lipid nanoparticles by differential scanning calorimetry. Int. J. Pharm. 304, 231–238.

Danielson, K.G., Anderson, L.W., Hosick, H.L., 1980. Selection and characterization in culture of mammary tumor cells with distinctive growth properties in vivo. Cancer Res. 40, 1812–1819.

Dong, X., Mattingly, C.A., Tseng, M., Cho, M., Adams, V.R., Mumper, R.J., 2009. Development of new lipid-based paclitaxel nanoparticles using sequential simplex optimization. Eur. J. Pharm. Biopharm. 72, 9–17.

Freitas, C., Muller, R.H., 1998. Effect of light and temperature on zeta potential and physical stability in solid lipid nanoparticles (SLN) dispersions. Int. J. Pharm. 168, 221–229.

Goldstein, J.L., Brown, M.S., 1990. Regulation of the mevalonate pathway. Nature 343, 425–430.

Graaf, M.R., Richel, D.J., van Noorden, C.J., Guchelaar, H.J., 2004. Effects of statins and farnesyltransferase inhibitors on the development and progression of cancer. Cancer Treat. Rev. 30, 609–641.

Heurtault, B., Saulnier, P., Pech, B., Proust, J.E., Benoit, J.P., 2003. Physico-chemical stability of colloidal lipid particles. Biomaterials 24, 4283–4300.

Hobbs, S.K., Monsky, W.L., Yuan, F., Roberts, W.G., Griffith, L., Torchilin, V.P., Jain, R.K., 1998. Regulation of transport pathways in tumor vessels: role of tumor type and microenvironment. Proc. Natl. Acad. Sci. U.S.A. 95, 4607–4612.

Jenning, V., Mader, K., Gohla, S.H., 2000. Solid lipid nanoparticles (SLN) based on binary mixtures of liquid and solid lipids: a (1)H-NMR study. Int. J. Pharm. 205, 15–21.

Kaneko, I., Hazama-Shimada, Y., Endo, A., 1978. Inhibitory effects on lipid metabolism in cultured cells of ML-236B, a potent inhibitor of 3-hydroxy-3-methylglutaryl-coenzyme-A reductase. Eur. J. Biochem. 87, 313–321.

Kotamraju, S., Williams, C.L., Kalyanaraman, B., 2007. Statin-induced breast cancer cell death: role of inducible nitric oxide and arginase-dependent pathways. Cancer Res. 67, 7386–7394.

Koyuturk, M., Ersoz, M., Altiok, N., 2007. Simvastatin induces apoptosis in human breast cancer cells: p53 and estrogen receptor independent pathway requiring signalling through JNK. Cancer Lett. 250, 220–228.

Lai, F., Wissing, S.A., Muller, R.H., Fadda, A.M., 2006. Artemisia arborescens L essential oil-loaded solid lipid nanoparticles for potential agricultural application: preparation and characterization. AAPS PharmSciTech 7, E2.

Ma, P., Dong, X., Swadley, C.L., Gupte, A., Leggas, M., Ledebur, H.C., Mumper, R.J., 2009. Development of idarubicin and doxorubicin solid lipid nanoparticles to overcome Pgp-mediated multiple drug resistance in leukemia. J. Biomed. Nanotechnol. 5, 151–161.

Maltese, W.A., Defendini, R., Green, R.A., Sheridan, K.M., Donley, D.K., 1985. Suppression of murine neuroblastoma growth in vivo by mevinolin, a competitive inhibitor of 3-hydroxy-3-methylglutaryl-coenzyme A reductase. J. Clin. Invest. 76, 1748–1754.

McIntyre, B.S., Briski, K.P., Gapor, A., Sylvester, P.W., 2000a. Antiproliferative and apoptotic effects of tocopherols and tocotrienols on preneoplastic and neoplastic mouse mammary epithelial cells. Proc. Soc. Exp. Biol. Med. 224, 292–301.

McIntyre, B.S., Briski, K.P., Tirmenstein, M.A., Fariss, M.W., Gapor, A., Sylvester, P.W., 2000b. Antiproliferative and apoptotic effects of tocopherols and tocotrienols on normal mouse mammary epithelial cells. Lipids 35, 171–180.

Muller, R.H., Radtke, M., Wissing, S.A., 2002. Nanostructured lipid matrices for improved microencapsulation of drugs. Int. J. Pharm. 242, 121–128.

Pasqualini, R., Arap, W., McDonald, D.M., 2002. Probing the structural and molecular diversity of tumor vasculature. Trends Mol. Med. 8, 563–571.

Samant, G.V., Sylvester, P.W., 2006. gamma-Tocotrienol inhibits ErbB3-dependent PI3K/Akt mitogenic signalling in neoplastic mammary epithelial cells. Cell. Prolif. 39, 563–574.

Sassano, A., Platanias, L.C., 2008. Statins in tumor suppression. Cancer Lett. 260, 11–19.

Schwarz, C., Mehnert, W., Lucks, J.S., Muller, R.H., 1994. Solid lipid nanoparticles (SLN) for controlled drug delivery. I. Production, characterization and sterilization. J. Control. Release 30, 83–96.

Serpe, L., Catalano, M.G., Cavalli, R., Ugazio, E., Bosco, O., Canaparo, R., Muntoni, E., Frairia, R., Gasco, M.R., Eandi, M., Zara, G.P., 2004. Cytotoxicity of anticancer drugs incorporated in solid lipid nanoparticles on HT-29 colorectal cancer cell line. Eur. J. Pharm. Biopharm. 58, 673–680.

Shah, S., Sylvester, P.W., 2004. Tocotrienol-induced caspase-8 activation is unrelated to death receptor apoptotic signaling in neoplastic mammary epithelial cells. Exp. Biol. Med. (Maywood) 229, 745–755.

Shah, S., Gapor, A., Sylvester, P.W., 2003. Role of caspase-8 activation in mediating vitamin E-induced apoptosis in murine mammary cancer cells. Nutr. Cancer 45, 236–246.

Shibata, M.A., Kavanaugh, C., Shibata, E., Abe, H., Nguyen, P., Otsuki, Y., Trepel, J.B., Green, J.E., 2003. Comparative effects of lovastatin on mammary and prostate oncogenesis in transgenic mouse models. Carcinogenesis 24, 453–459.

Souto, E.B., Mehnert, W., Muller, R.H., 2006. Polymorphic behaviour of Compritol888 ATO as bulk lipid and as SLN and NLC. J. Microencapsul. 23, 417–433.

Teeranachaideekul, V., Souto, E.B., Junyaprasert, V.B., Muller, R.H., 2007. Cetyl palmitate-based NLC for topical delivery of coenzyme Q(10)—development, physicochemical characterization and in vitro release studies. Eur. J. Pharm. Biopharm. 67, 141–148.

Thibault, A., Samid, D., Tompkins, A.C., Figg, W.D., Cooper, M.R., Hohl, R.J., Trepel, J., Liang, B., Patronas, N., Venzon, D.J., Reed, E., Myers, C.E., 1996. Phase I study of lovastatin, an inhibitor of the mevalonate pathway, in patients with cancer. Clin. Cancer Res. 2, 483–491.

Wali, V.B., Sylvester, P.W., 2007. Synergistic antiproliferative effects of gamma-tocotrienol and statin treatment on mammary tumor cells. Lipids 42, 1113–1123.

Wali, V.B., Bachawal, S.V., Sylvester, P.W., 2009. Combined treatment of gamma-tocotrienol with statins induce mammary tumor cell cycle arrest in G1. Exp. Biol. Med. (Maywood) 234, 639–650.

Wong, H.L., Bendayan, R., Rauth, A.M., Li, Y., Wu, X.Y., 2007. Chemotherapy with anticancer drugs encapsulated in solid lipid nanoparticles. Adv. Drug Deliv. Rev. 59, 491–504.

Yuan, H., Miao, J., Du, Y.Z., You, J., Hu, F.Q., Zeng, S., 2008. Cellular uptake of solid lipid nanoparticles and cytotoxicity of encapsulated paclitaxel in A549 cancer cells. Int. J. Pharm. 348, 137–145.